Time-of-Flight Secondary Ion Mass Spectrometry Imaging Demonstrates the Specific Localization of Deca-Bromo-Diphenyl-Ether Residues in the Ovaries and Adrenal Glands of Exposed Rats

Alexandre Seyer,[a] Anne Riu,[b] Laurent Debrauwer,[b] Nathalie Bourgès-Abella,[c] Alain Brunelle,[a] Olivier Laprévote,[a,d] and Daniel Zalko[b]

[a] Centre de recherche de Gif, Institut de Chimie des Substances Naturelles, CNRS, Gif-sur-Yvette, France
[b] UMR 1089 Xénobiotiques INRA-ENVT, Toulouse, France
[c] Département des Sciences Cliniques, École Nationale Vétérinaire de Toulouse, Toulouse, France
[d] Chimie Toxicologie Analytique et Cellulaire, EA 4463, Faculté des Sciences Pharmaceutiques et Biologiques, Université Paris Descartes, Paris, France

Deca-bromo-diphenyl ether (DBDE) is one of the most efficient brominated flame retardant (BFR) available on the market. We recently demonstrated that when administered to female rat by oral route, DBDE is efficiently absorbed, with the highest residual concentrations found in two endocrine glands, namely the adrenal glands and the ovaries. Time-of-flight secondary ion mass spectrometry (TOF-SIMS) imaging, a technique usually used for the study of endogenous compounds, was applied for the first time to a persistent organic pollutant, allowing to detect and to precisely localize DBDE residues in these two target tissues. The detection of the bromide ion (^{81}Br isotope) by TOF-SIMS mass spectrometry imaging allowed us to demonstrate a marked cortical tropism of DBDE residues for the adrenal glands in female rats dosed per os 2 $mg \cdot kg^{-1}$ DBDE, daily, over 96 h. In ovaries, DBDE residues were found to be concentrated in spots corresponding to part of the corpora lutea. Hepatic residues of DBDE were found to be homogeneously distributed. Due to the intrinsic toxicity of DBDE, its accumulation in the adrenal glands and the ovaries may be connected to the mechanisms of actions by which DBDE could trigger endocrine disruption in mammals. (J Am Soc Mass Spectrom 2010, 21, 1836–1845) © 2010 American Society for Mass Spectrometry

Polybromo diphenyl ethers (PBDE) are a major class of brominated flame retardants (BFR). They are widely used to manufacture various industrial and domestic devices, with the aim to prevent or minimize fire damage. PBDE have been demonstrated to be present in the environment [1, 2], in animals [3, 4], as well as in human tissues [5, 6]. Among the three different formulations of PBDEs that are currently manufactured ("penta", "octa", and "deca"), the "deca-mix" is the most widely used, and is nowadays in many countries the only mix that remains marketed [7]. Deca-BDE (DBDE) is the major constituent (ca. 97%) of the "deca" commercial mix. Lower molecular weight PBDE (tetra-BDE to hepta-BDE) are the compounds that have been the most extensively studied. It has been demonstrated that some of them can induce neurotoxic effects in mice [8, 9]. They are suspected to impact thyroid hormonal regulation [10], and display agonist and antagonist activities towards the Ah receptor [11]. They also induce the expression of CYP1A1 and CYP1A2 [12], which are proteins that belong to the cytochrome P450 superfamily and are involved in the metabolism of exogenous as well as endogenous molecules such as steroids. DBDE was considered by manufacturers to be poorly bioavailable (below 1%) due to its high molecular weight [13], and only a limited number of studies have examined its toxicity.

Because of technical difficulties, higher brominated PBDEs are seldom monitored in studies dealing with human exposure. However, when they are, DBDE and other high molecular weight PBDE are major contaminants [14]. For instance, in humans, the presence of DBDE has been reported in mother's milk [15], serum [16, 17] and adipose tissue [14, 18, 19]. These conclusions are also supported by recent data obtained in rat using radio-labeled [^{14}C]-DBDE [20, 21], which demonstrate that DBDE bioavailability is above 20%. Its residues have been shown to markedly concentrate in the

Address reprint requests to Dr. A. Brunelle, Institut de Chimie des Substances Naturelles, CNRS, Avenue de la Terrasse, F-91198 Gif-sur-Yvette, France. E-mail: Alain.Brunelle@icsn.cnrs-gif.fr

1044-0305/10/$32.00
doi:10.1016/j.jasms.2010.06.019

Published online July 7, 2010
Received April 14, 2010
Revised June 25, 2010
Accepted June 26, 2010

liver and the adrenal glands [20, 21] as well as in the ovaries [21]. Of particular interest is the fact that DBDE respective residual concentrations are even higher in these two endocrine glands than in the liver itself. In rats dosed 2 $mg \cdot kg^{-1}$ labeled DBDE, residual levels were 11.2, 16.1 and 33.0 ppm in the liver, the ovaries, and the adrenal glands, respectively. Moreover, part of the detected radioactivity (about 10% in adrenal glands and ovaries) was found to be associated with debrominated metabolites. This debromination may result in the bioactivation of PBDE, the structure of which is relatively close to that of poly-chlorinated biphenyls (PCBs) and dioxins. PBDE metabolites such as hydroxylated tetra-BDE have been shown to be endocrine disrupting chemicals (EDCs) [22, 23]. Thus, the consequences of the presence of these residues in endocrine glands needs to be better understood, beginning with the study of their precise localization. We consequently decided to use mass spectrometry imaging (MSI), namely time-of-flight secondary ion mass spectrometry (TOF-SIMS) imaging, to localize DBDE residues in the liver as well as in the two main target tissues of DBDE in female rats: the adrenal glands and the ovaries.

MALDI-TOF [24] and nano-SIMS [25] are two mass spectrometry methods that are frequently used for imaging. MALDI-TOF mass spectrometry imaging is able to detect numerous classes of molecules (lipids, metabolites, peptides, proteins . . .) with the possibility to perform in situ tandem mass spectrometry experiments, but with a spatial resolution limited to 50 μm. This would not allow localizing the compounds with enough precision. Nano-SIMS imaging can detect elements with a spatial resolution of a few tens of nanometers. However, the field of view is only of several tens of micrometers, which would not have enabled to record the image of entire organs. Moreover, sample preparation methods for nano-SIMS are relatively difficult and long to implement. Finally, taking into account the size of the tissues to be analyzed in the present study (a few millimeters), the use of nano-SIMS or MALDI-TOF MSI would have led to very long acquisition times.

Until recently, the mass to charge ratio (m/z) of the ions that could be imaged using TOF-SIMS instrument was limited to 100–200, mainly because the ion sources used were inefficient in transferring intact heavy molecular ions into the gas phase. The range of biological applications was therefore relatively limited [26]. Nowadays, thanks to the increase of sensitivity due to advent of polyatomic ion beams such as those of gold [27–29], bismuth [30], or C_{60} fullerenes [31], the field of TOF-SIMS imaging has been greatly extended. This method now enables drawing from various kinds of samples the density map (image) of any ion present in the mass spectra, with a spatial resolution from a few μm to less than 500 nm, and with a mass range which is now reaching more than 1000 Da. In recent years, many applications of TOF-SIMS imaging have been published in the fields of biology and medicine [32–43]. However, it has never been directly applied to the exploration of persistent organic pollutants such as environmental or food contaminants.

Thus, TOF-SIMS imaging appeared to be the best suited method to map DBDE in the liver, the adrenal glands, and the ovaries of orally dosed rats, following the in vivo experimental conditions already used by Riu et al. [21], but using non-radio-labeled DBDE. Histologic studies of the imaged tissue sections were carried out in parallel to TOF-SIMS imaging, with the aim to better understand the tissue distribution of DBDE residues.

Experimental

Female Wistar rats, aged 12 wk ($n = 6$), were acclimatized with a 12/12 h light/dark cycle for 1 wk and were fed a standard diet with ad libitum access to water. Three animals were force-fed, during 4 consecutive d, a daily dose of 2 $mg \cdot kg^{-1}$ DBDE (Sigma, Saint-Quentin-Fallavier, France) dissolved in peanut oil as described previously [21]. Three animals were forced-fed only with peanut oil (control). Animals were euthanized by cervical dislocation followed by exsanguinations 24 h after the last DBDE dosage. The liver, the adrenal glands, and ovaries were removed and immediately frozen and stored at −80 °C until time of analysis.

Sections were made with a CM3050-S cryostat (Leica Microsystems SA, Nanterre, France) at −20 °C for the adrenal glands and the liver, and at −25 °C for ovaries. Cryostat sections (10 μm for adrenal glands and ovaries; 14 μm for the liver) were immediately collected on a silicon wafer (2 in. diameter polished silicon wafers; ACM, Villiers-Saint-Frédéric, France). After each ovary section, an adjacent section was made and collected on a glass slide for Masson's trichrome histologic staining (Sigma Kit HT15; Saint-Quentin-Fallavier, France). Before analysis, cryostat sections were dried under a pressure of a few hectopascals for 10 min. Optical images were recorded from both silicon wafer and glass slide sections using a photonic BX51 microscope fitted with ×1.25 to ×50 objectives (Olympus, Rungis, France) coupled to a Color View I camera monitored by Cell^{B} software (Soft Imaging System GmbH, Münster, Germany).

All ion images were recorded with a TOF-SIMS IV commercial mass spectrometer (Ion-Tof GmbH, Münster, Germany) located at the Institut de Chimie des Substances Naturelles in Gif-sur-Yvette (France). This mass spectrometer is fitted with a bismuth liquid metal ion gun (LMIG) delivering Bi_n^{q+} bismuth cluster ions (Bi_3^+ ions were selected). Primary ions reached the sample surface with a kinetic energy of 25 keV and an angle of incidence of 45°. The primary ion dose density used for the experiments was set between 6×10^{10} and 9×10^{10} ions $\cdot$ cm^{-2}, well below the static SIMS limit [44]. This ion dose was chosen to limit both the acquisition time to 6 h and the size of the raw data files to ca. 1.5 Gb. Secondary ions were accelerated to a kinetic

energy of 2 keV, passed through a field free region and a single-stage reflectron (first-order compensation). The effective ion flight path was ~2 m. Ions were then post-accelerated to a kinetic energy of 10 keV before hitting a hybrid detector composed by a microchannel plate, a scintillator, and a photomultiplier. A low-energy electron flood gun was activated between two primary ion pulses to neutralize the sample surface. In this study, we used the so-called "high current bunched mode" to set the primary ion column [45]. This mode of operation allows reaching a spatial resolution of 2 μm, while maintaining an excellent mass resolution of about $M/\Delta M = 8 \times 10^3$ (FWHM) at *m/z* 500, and a pulsed primary ion current (measured with a Faraday cup located on the grounded sample holder) of 0.35 pA for Bi_3^+ at 10 kHz, which does not penalize the time required for ion images acquisition. Because of the very low initial kinetic energy distribution of the secondary ions, the relation between time-of-flight and the square root of the mass-to-charge ratio *m/z* is always linear. Consequently the mass spectra were always internally calibrated using signals from C^-, CH^-, CH_2^-, C_2^-, C_3^-, and C_4H^- ions, in the negative ion mode. The so-called "stage scan" raster mode was used. In this mode, the sample is continuously moved by the sample stage in a saw-tooth mode and scans the whole surface area. The primary ion beam is rastering itself inside the area of each individual pixel. The time required to achieve one analysis with this mode is about 6 h, mainly because of the positioning control of the sample holder. Images were always recorded with a number of pixels equal to 256 × 256, meaning that the pixel size varied with the size of the area to be analyzed. For example, an area of 8×8 mm^2 would result in a pixel size of 31.25×31.25 μm^2.

Results and Discussion

The TOF-SIMS mass spectrum, recorded in the negative ion mode from a solution of DBDE (1 mg · mL^{-1}) is shown in Figure 1. A very weak signal corresponding to the molecular ion ($M^{-\cdot}$, *m/z* 959.19 for the $^{79}Br_5$ $^{81}Br_5$ isotopomer) was detected, showing that the detection of this molecule based on the monitoring of the molecular ion at the surface of a tissue section would be extremely difficult. Besides the $M^{-\cdot}$ ions, several brominated isotopic clusters corresponding to the fragmentation of the molecular ion via bromine atoms eliminations were detected. These were centered on the *m/z* 878.10, 798.21, and 718.29 ion peaks, respectively. The spectrum (Figure 1) also displayed the $C_6Br_5O^-$ fragment ion (isotopic pattern ranging from *m/z* 482.52, $^{12}C_6{}^{79}Br_5{}^{16}O^-$ to 492.52, $^{12}C_6{}^{81}Br_5{}^{16}O^-$) generated by the cleavage of the ether bond of the molecule. Conversely, the Br^- (*m/z* 78.91 and 80.91), Br_2^- (*m/z* 157.82, 159.81, 161.82) and Br_3^- (*m/z* 236.71, 238.71, 240.72 and 242.71) ion peaks were by far the most intense signals, the Br^- ions being the base peak of the spectrum. The ion peaks corresponding to the two natural isotopes of bromine, and displaying almost the same natural abundances (50.69% and 49.31%, respectively), were the only ones detected in organs of dosed rat. They were never detected in organs of control rat (Figure 2). The $^{79}Br^-$ isotope was detected at *m/z* 78.906 (average of all experiments) with a deviation of 13 ppm (Table 1), compared with the theoretical mass-to-charge ratio (*m/z* 78.918). As shown in Figure 2, this peak was located at the left edge of a very intense peak corresponding to the phosphite ion PO_3^- (mean value *m/z* 78.961). The signal corresponding to this ion

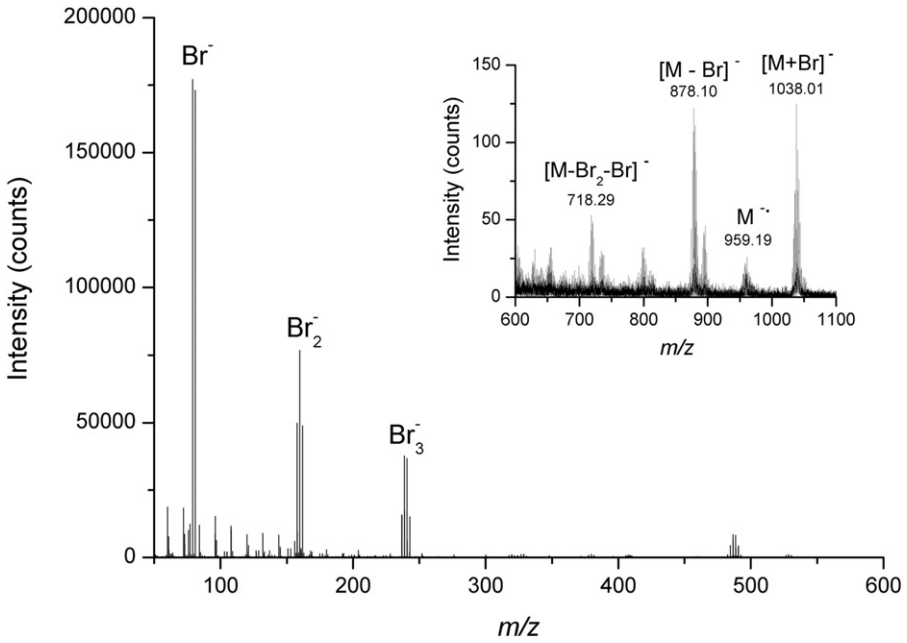

Figure 1. TOF-SIMS negative ion mass spectrum of a standard solution of deca-bromo-diphenyl ether at a concentration of 1 mg · mL^{-1} in methanol/water 50:50 vol:vol.

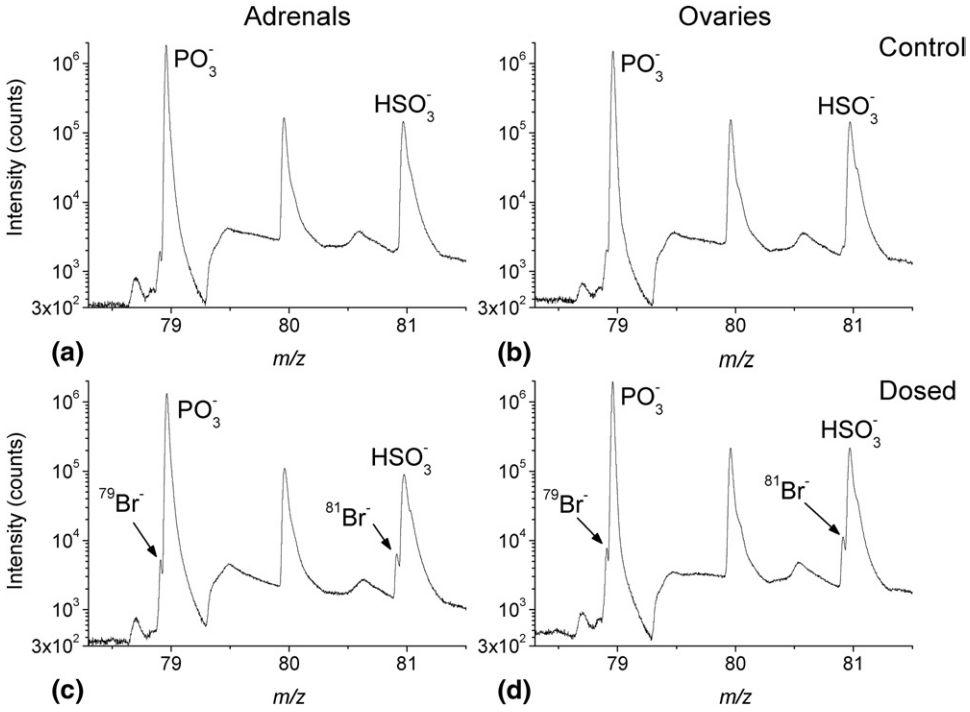

Figure 2. Parts of the TOF-SIMS negative ion mass spectra recorded at the surface of sections from adrenal glands of control (**a**) and dosed rat (**c**), and from ovaries of control (**b**) and dosed (**d**) rats. A log scale has been chosen for the *y*-axis to better show all the peaks with very different intensities.

was so intense that at least one ion was emitted at this mass-to-charge ratio after each primary ion pulse, leading to a very large and distorted peak due to the dead time of the entire electronic chain (constant fraction discriminator and time-to-digital converter) following the detector. This saturation is clearly evidenced in Figure 2 (for which the intensity on the *y*-axis was intentionally drawn using a log scale) by the average chemical noise level, which is falling down just after the intense PO_3^- ion peak. The very high intensity of this ion peak together with the close *m/z* ratio values of the PO_3^- and $^{79}Br^-$ ions can therefore explain the large error on the measured value of the $^{79}Br^-$ isotope mass-to-charge ratio. Since the PO_3^- ion signal is saturated, this ion appears as homogeneously distributed over the entire ion image and thus makes false the representation of the $^{79}Br^-$ ion image. The situation was different for the $^{81}Br^-$ isotope (theoretical mass 80.916 Da) which was detected at *m/z* 80.910, with a mass deviation of 7 ppm. This ion peak was also located at the left edge of an intense ion peak, i.e., the bisulphite HSO_3^- ion peak (*m/z* 80.974). Nevertheless, in this case, the HSO_3^- ion peak is much less intense than the PO_3^- ion peak (see Figure 2). The corresponding signal was consequently not saturated, and did not disturb the ion image of the $^{81}Br^-$ ion, thanks to a better separation of the two peaks. Figure S1, which can be found in the electronic version of this article, shows that $^{81}Br^-$ and HSO_3^- ions have different spatial distributions, while the distributions of $^{79}Br^-$ and PO_3^- ions cannot be differentiated since the PO_3^- ion signal is saturated (its ion image is uniform and cannot exhibit any contrast).

An improved separation between these two close ion peaks could be achieved by making the secondary ions fly in the field-free path of the TOF-SIMS IV mass spectrometer with a kinetic energy of 1 keV, instead of 2 keV. This was obtained by maintaining the extraction voltage at 2 kV and by decelerating the secondary ions only when entering the field-free path. The post-acceleration before the detector was kept at 10 kV. Neither the extraction of the secondary ions nor their detection efficiency was affected. Using this method, both the time-of-flight and the separation of all the ions were increased by a factor of square root of two. Figure 3

Table 1. Mass-to-charge ratio of $^{79}Br^-$ and $^{81}Br^-$ bromide ions measured by TOF-SIMS at the surface of sections from ovaries and adrenal glands of dosed rats and their deviation in ppm regarding to the exact mass

	$^{79}Br^-$	Dev (ppm)	$^{81}Br^-$	Dev (ppm)
Theoretical *m/z*	78.918		80.916	
Experimental *m/z* (measured on adrenal gland sections)	78.908	11	80.911	5
Experimental *m/z* (measured on ovary sections)	78.904	14	80.909	7
Experimental *m/z* (mean value from the two organs)	78.906	13	80.909	7

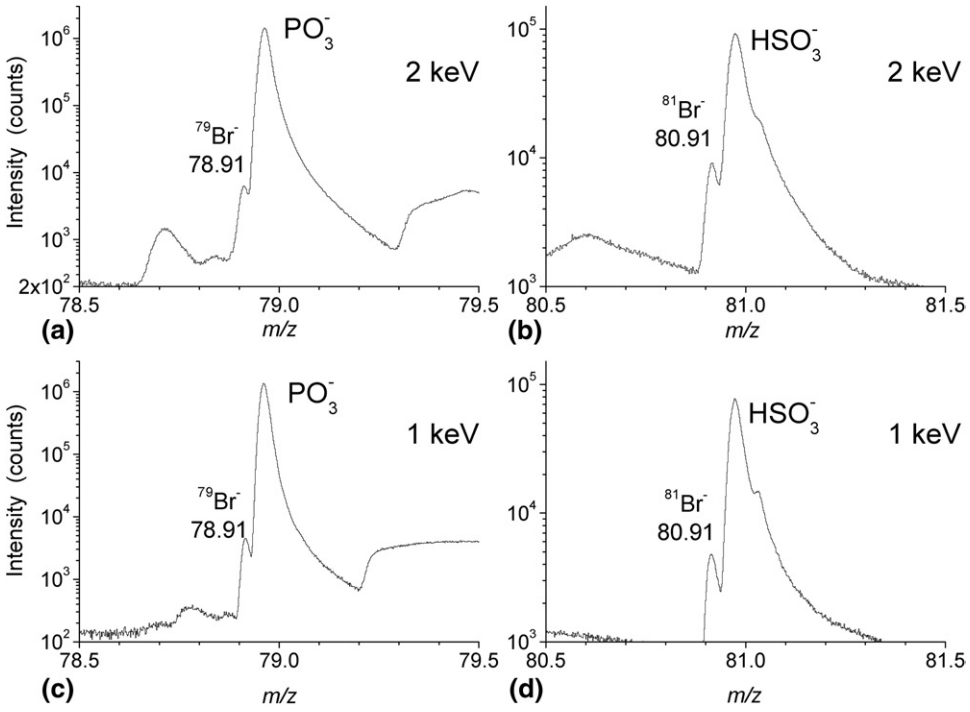

Figure 3. Parts of the TOF-SIMS negative ion mass spectra recorded at the surface of sections from adrenal glands of a dosed rat for 2 keV (**a**) and (**b**) and 1 keV (**c**) and (**d**) of secondary ion kinetic energy.

shows parts of the spectra obtained at the surface of an adrenal gland section from a dosed rat, with kinetic energies of 2 keV (top) and 1 keV (bottom), respectively. The use of 1 keV kinetic energy led to a better mass separation between each of the two bromide isotopes and the PO_3^- and HSO_3^- ions, respectively, as indicated in Figure 3c and d. Nevertheless the intensity of the $^{81}Br^-$ ion peak was diminished by a factor of 2.7 when decreasing the secondary ion kinetic energy because this option led to a fall down in the transmission of the time-of-flight analyzer. Regarding the separation of the $^{79}Br^-$ and PO_3^- ions, the separation's enhancement was not sufficient to get rid of the mix between the two ions· Consequently, these low-energy settings of the analyzer were not selected for the studies, and only the $^{81}Br^-$ isotopic ion was used for the imaging of DBDE residues at the surface of adrenal gland and ovary sections of dosed rats. Since the natural abundance of this isotope accounts for nearly half of the total amount of bromine in the samples, these difficulties in the measurements did not affect the worthiness of the results.

Following the optimization of the method, we proceeded to the TOF-SIMS imaging of tissues of organs from rats exposed in vivo to DBDE versus controls. Given the technical impossibility to base on the signal directly corresponding to DBDE, we did not aim to distinguish between the parent compound and its metabolites. However, it was previously demonstrated that the main part of the extractible radioactivity found in the adrenal glands and the ovaries of rats dosed orally with DBDE in these in vivo conditions does primarily correspond to unchanged DBDE, while metabolites (lower brominated PBDE congeners) account only for roughly 10% of the overall residues [21].

Bromide ions were detected in hepatic parenchyma, where they presented a homogeneous distribution, which prevented spotting a specific localization such as periportal or centrolobular zonation (data not shown). Images recorded from one quarter of the surface of adrenal gland sections of dosed and control rats are presented in Figure 4. The left column (Figure 4a, b, and c) shows optical images on which the red color squares indicate the areas analyzed by TOF-SIMS imaging. The middle column (Figure 4d, e, and f) shows the $^{81}Br^-$ ion images recorded from adrenal sections of dosed rats, and the right column (Figure 4g, h, and i) shows the ion images of the $^{81}Br^-$ ion peak recorded from adrenal sections of control rats. Dosed and control rats $^{81}Br^-$ images (d and g, e and h, f and i, respectively) in Figure 4 were generated by selecting exactly the same area. In dosed rats, the bromide ion was clearly detected in the cortex of the adrenal glands. The bromide ion distribution appeared heterogeneous even if it seemed that its main localization was the outer cortex containing cells with cytoplasmic lipid droplets enriched in aldosterone (zona glomerulosa) and corticosterone (zona fasciculata). In contrast, in control animals, no significant amount and specific location of the bromide ion was detected. Although the occurrence of ion suppression effects or "matrix effects" can not be totally ruled out, the comparison of the images obtained on the dosed rats with those obtained on the control ones, and the

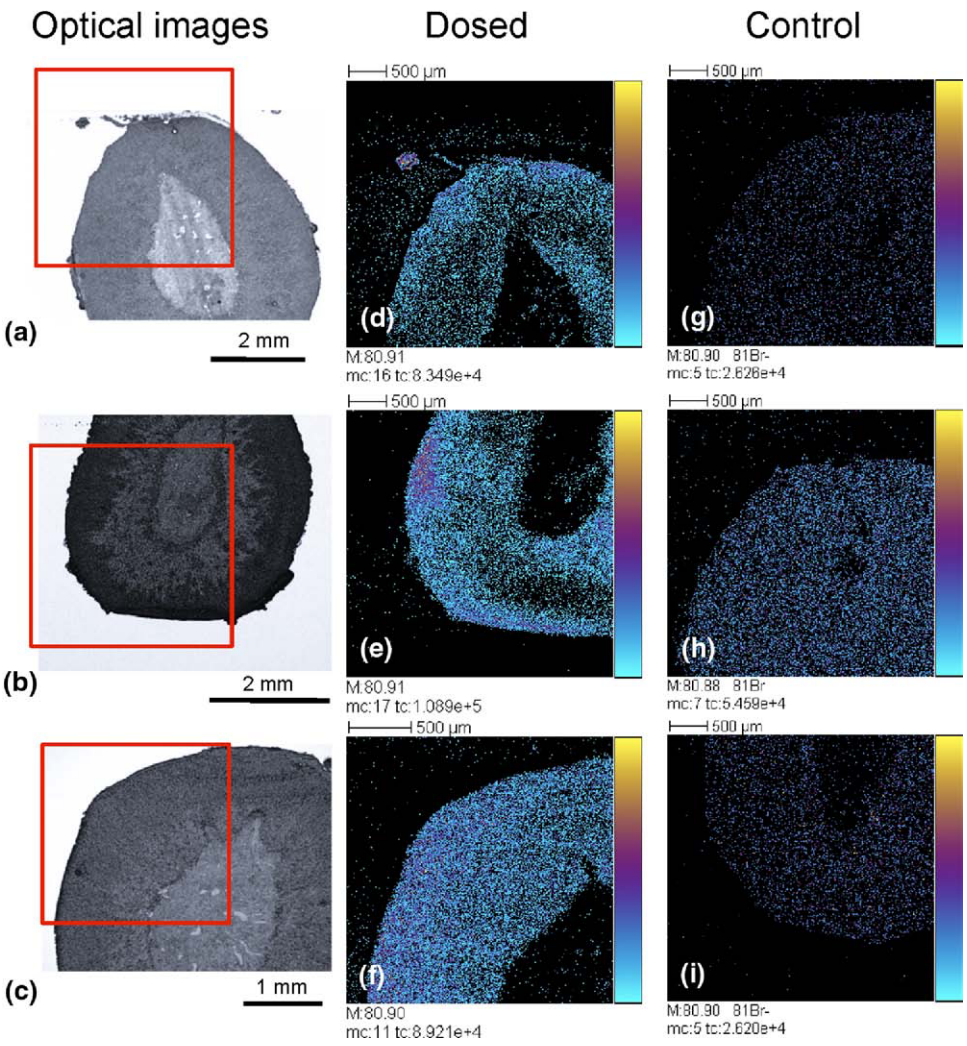

Figure 4. TOF-SIMS negative ion images recorded at the surface of sections from adrenal glands of rats. (**a**), (**b**), (**c**): optical images of sections from adrenal glands of dosed rats. The red squares indicate the areas from which the ion images (**d**), (**e**), and (**f**) were recorded. (**d**), (**e**), (**f**): $^{81}Br^-$ ion, dosed rats. (**g**), (**h**), (**i**): control rats, images were obtained after the selection, in the mass spectra, of the same window as for the $^{81}Br^-$ ion. For all ion images: field of view 3.52 × 3.52 mm^2; 256 × 256 pixels, pixel size 13.75 μm^2, 512 shots/pixel, fluence: 8 × 10^{10} ions · cm^{-2}. Color scale bars, with amplitude in number of counts, are indicated to the right of each ion image. The amplitude of the color scale corresponds to the maximum number of counts *mc* indicated below each ion image, and could be read as [0, *mc*]; *tc* is the total number of counts recorded for the specified *m/z* (sum of counts in all the pixels).

optical images clearly shows a tropism of brominated species for particular zones of the organs studied. For the latter animals, it can then be considered that the low intensity signals recorded in the adrenal (g, h, and i images: controls) only correspond to the HSO_3^- ion contribution at the base of the $^{81}Br^-$ ion peak, constituting a background signal. Moreover, it is important to notice that when the bromide ion is detected (middle column) the amplitude *mc* of the color scale of each image is greater than when not detected (right column).

The structure of PBDE is closely related to that of PCBs, for which the toxicity was largely documented in particular as endocrine disruptors [22, 23]. Among others, it has been demonstrated that PCBs and some of their hydroxylated metabolites target the adrenal glands of marine mammals, inducing the hyperplasia of the cortical area [46]. The immunotoxicity of PCBs was demonstrated in another study with rats, which is consistent with the known deregulation of the immune system by corticosteroids [47]. In the case of PCBs, cortical hyperplasia of the adrenal glands is hypothesized to be correlated with an increased production of cortisol, which in turn triggers the down regulation of the immune system. Given the structural similarity between PCBs and PBDEs, it is noteworthy that DBDE residues mainly target the outer part of the adrenal cortex. Why these residues specifically accumulate in this part of the adrenal glands while, in contrast, the

medulla is not a target for DBDE, remains to be better understood. Though the current knowledge about the toxicity of DBDE is insufficient to link BFR exposure to adverse outcomes due to a disruption of the adrenocortical function, this hypothesis is greatly favored by the conclusions of TOF-SIMS imaging. Further in vivo exploration studies of the adrenal function will be necessary to confirm this hypothesis.

Images recorded on ovary sections of dosed and control rats are presented in Figure 5. The layout of this figure is the same as for Figure 4. The left column shows ovary micrographies recorded after Masson's trichrome staining (Figure 5a, b, and c). The medium column presents the $^{81}Br^-$ ion images recorded from ovary sections of dosed rats (Figure 5d, e, and f) while right column shows images from control rats. The bromide ions appeared to accumulate in only part of the several corpora lutea observed in the ovarian stroma from dosed rats, while others were not colored. This result could be explained by the fact that all corpora lutea were not at the same stage of development. In species like rat, which have a 4-d long estrous cycle, luteal cells

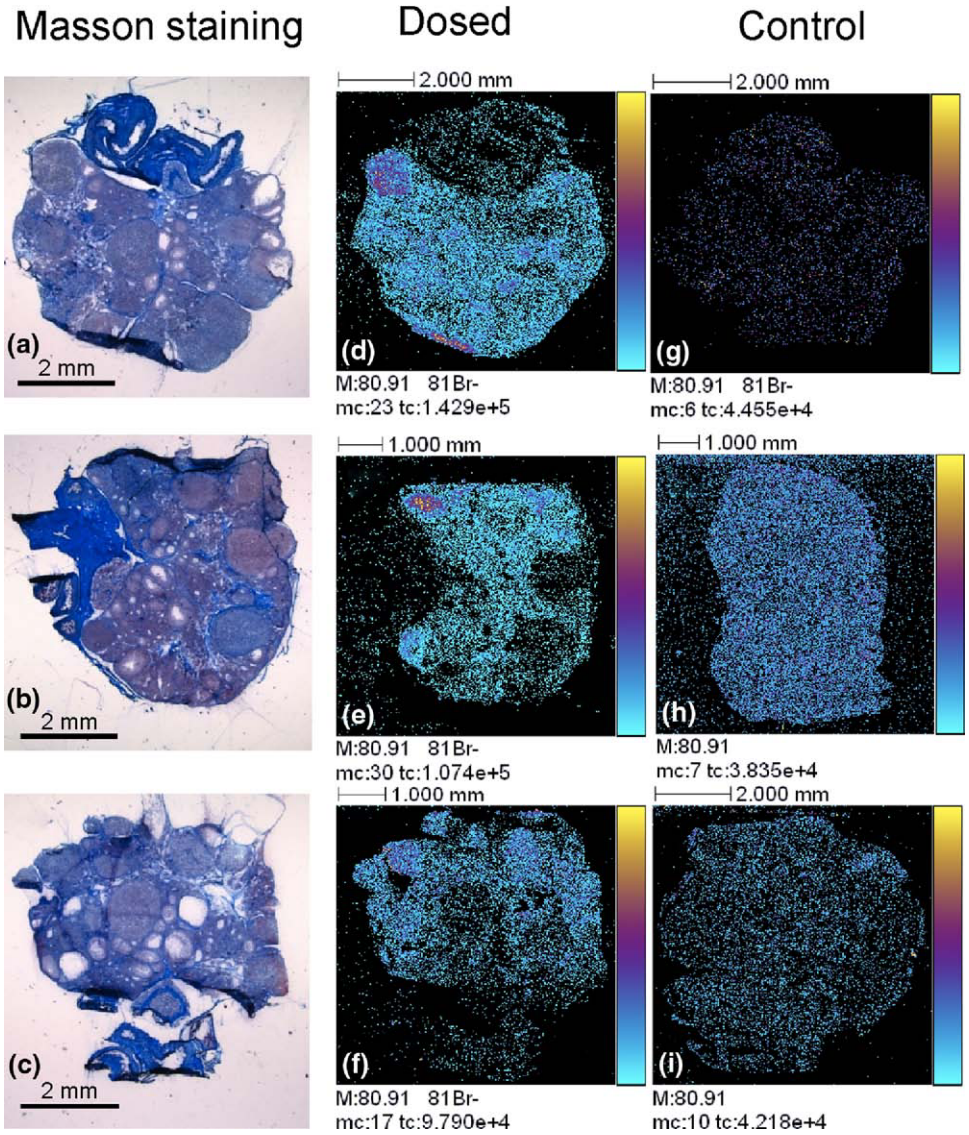

Figure 5. TOF-SIMS negative ion images recorded at the surface of sections from ovaries of rats. (**a**), (**b**), (**c**): Optical images of trichrome Masson staining of ovaries sections of dosed rats. The collagenic dense ovarian stroma was stained in blue whereas ovarian follicles and corpora lutea show as pink ovoid structures. (**d**), (**e**), (**f**): $^{81}Br^-$ ion, dosed rats; (**g**), (**h**), (**i**): control rats, images were obtained after selection, in the mass spectra, of the same window as for the $^{81}Br^-$ ion. For all ion images: field of view 6×6 to 7.4×7.4 mm^2; 256×256 pixels, pixel size 23.4×23.4 μm^2 to 28.9×28.9 μm^2, 512 shots/pixel, fluence: from 1.8×10^{10} to 4×10^{10} ions $\cdot$ cm^{-2}. Color scale bars, with amplitude in number of counts, are indicated to the right of each ion image. The amplitude of the color scale corresponds to the maximum number of counts *mc* indicated below each ion image, and could be read as [0, *mc*]; *tc* is the total number of counts recorded for the specified *m/z* (sum of counts in all the pixels).

actively synthesize steroids, and progesterone-rich tiny lipid cytoplasmic droplets are present in corpora lutea only at the day of diestrus [48]. In the conditions suitable to enable TOF-SIMS imaging, the produced sections enabled a satisfactory histologic analysis, but did not allow to fully characterizing the histologic stage of corpora lutea. Like other organo–halogen compounds, including polybrominated biphenyls (PBB) and PCBs, PBDE are relatively lipid soluble xenobiotics. Compounds like PCB have been shown to adversely affect progesterone production [49]. It could therefore be hypothesized that DBDE (or its metabolites) present at the level of the corpora lutea may disrupt natural steroidogenesis in the ovary.

In these experiments, the maximum spatial resolution provided by TOF-SIMS mass spectrometry imaging was not fully implemented. Moreover, the primary ion dose of a few 10^{10} ions per cm^2 used to record the ion images shown in Figure 5 was several orders of magnitude below the so-called static SIMS limit. A second image was therefore recorded for specific areas of the same ovarian section. This is shown in Figure 6, where the $^{81}Br^-$ ion, which appeared to accumulate in Figure 5d, was mapped with a better spatial resolution and higher primary ion fluence. Figure 6a shows the optical image after Masson's trichrome staining from the dosed rat ovary section in which the red color square delimitates the analyzed area. Figure 6b shows the $^{81}Br^-$ ion image, and Figure 6c the same image after a reduction of the number of pixels from 256 × 256 to 128 × 128, the intensity of each pixel now corresponding to the sum of four adjacent pixels. This method allowed in the present case to improve the apparent contrast of images, at the expense of a reduction of the spatial resolution by a factor of 2. This additional magnified acquisition clearly confirmed the localization of the bromide ion in the corpus luteum.

Conclusion

TOF-SIMS imaging using a bismuth cluster ions source allowed for the first time and with a high precision to localize the residues of a xenobiotic of large toxicological interest, namely the brominated flame retardant DBDE, at the level of its target tissues. DBDE was spotted in well-defined parts of two endocrine glands, as demonstrated by in vivo experiments carried out in rat as a model animal. Although DBDE was not detected in its molecular form, it was possible to map it at the surface of adrenal glands and ovaries thanks to the detection of the $^{81}Br^-$ isotope of the bromide ion, which was only detected in organs from dosed rats. This ion was located in the cortical area of adrenal glands. Despite the low amount of work documenting BFR's effects, this appears to be consistent with the several studies that previously demonstrated a link between PCB exposure and cortical hyperplasia (as well as related immunotoxic effects). Indeed, these organo–halogen compounds are very close to DBDE in terms of chemical structure. In ovaries from dosed rat, the $^{81}Br^-$ ion was detected in active corpora lutea, which is even more alarming than the previously released data demonstrating that, quantitatively, ovaries are the second main target tissue of DBDE in rat [21]. Given the fact that some PBDE metabolites have been shown to act as nuclear receptor ligands [10], TOF-

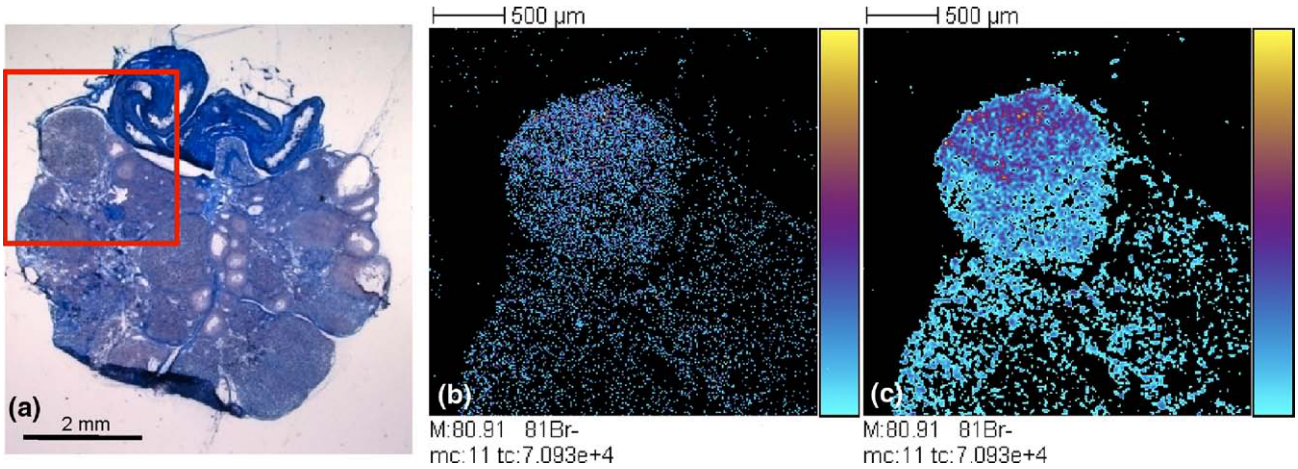

Figure 6. Precise localization of $^{81}Br^-$ in rat ovary. (**a**) Optical image of trichrome Masson staining of an ovary section of dosed rat. The red square indicates the area in which the ion image was recorded. (**b**) TOF-SIMS negative ion images of the $^{81}Br^-$ ion recorded at the surface of a section from an adrenal of dosed rat. (**c**) Same image as (**b**), but after having summed the number of counts of all four adjacent pixels. Field of view 2.7 × 2.7 mm^2, 256 × 256 pixels, pixel size 10.5 × 10.5 μm^2 (**b**) and 128 × 128 pixels, pixel size 21 × 21 μm^2 (**c**), 512 shots/pixel, fluence 1.4×10^{11} ions · cm^{-2}. Color scale bars, with amplitude in number of counts, are indicated to the right of each ion image. The amplitude of the color scale corresponds to the maximum number of counts *mc* and could be read as [0, *mc*]; *tc* is the total number of counts recorded for the specified *m/z* (sum of counts in all the pixels).

SIMS imaging techniques could provide valuable data, enabling to better understand the possible endocrine disrupting effects of DBDE, as well as lower brominated PBDE.

Acknowledgments

The authors acknowledge support for this work by the European Union (contract LSHG-CT2005-518194 COMPUTIS). The Ph.D. research fellowship of A.S. is supported by the Institut de Chimie des Substances Naturelles (CNRS).

Appendix A
Supplementary Material

Supplementary material associated with this article may be found in the online version at doi:10.1016/j.jasms.2010.06.019.

References

1. Watanabe, I.; Kashimoto, T.; Tatsukawa, R. Confirmation of the Presence of the Flame-Retardant Decabromobiphenyl Ether in River Sediment from Osaka. *Jpn. B Environ. Contam. Tox.* **1986,** *36,* 839–842.
2. Yamamoto, H.; Okumura, T.; Nishikawa, Y.; Konishi, H. Determination of Decabromobiphenyl Ether in Water and Sediment Samples by Gas Chromatography with electron Capture Detection. *J. AOAC Int.* **1997,** *80,* 102–106.
3. Lindstrom, G.; Wingfors, H.; Dam, M.; von Bavel, B. Identification of 19 Polybrominated Diphenyl Ethers (PBDEs) in Long-Finned Pilot Whale (*Globicephala melas*) from the Atlantic. *Arch. Environ. Con. Tox.* **1999,** *36,* 355–363.
4. Huwe, J. K.; Lorentzsen, M.; Thuresson, K.; Bergman, A. Analysis of Mono- to Deca-Brominated Diphenyl Ethers in Chickens at the Part Per Billion Level. *Chemosphere* **2002,** *46,* 635–640.
5. Noren, K.; Meironyte, D. Certain Organochlorine and Organobromine Contaminants in Swedish Human Milk in Perspective of Past 20–30 Years. *Chemosphere* **2000,** *40,* 1111–1123.
6. Sjodin, A.; Jones, R. S.; Focant, J. F.; Lapeza, C.; Wang, R. Y.; McGahee, E. E.; Zhang, Y. L.; Turner, W. E.; Slazyk, B.; Needham, L. L.; Patterson, D. G. Retrospective Time-Trend Study of Polybrominated Diphenyl Ether and Polybrominated and Polychlorinated Biphenyl Levels in Human Serum from the United States. *Environ. Health Persp.* **2004,** *112,* 654–658.
7. EHC-162. Environmental Health Criteria 162. Brominated Diphenyl ethers. International Program on Chemical Safety. World Health Organization: Geneva, Switzerland; 1994.
8. Eriksson, P.; Viberg, H.; Jakobsson, E.; Orn, U.; Fredriksson, A. A Brominated Flame Retardant, 2,2′,4,4′,5-Pentabromodiphenyl Ether: Uptake, Retention, and Induction of Neurobehavioral Alterations in Mice During a Critical Phase of Neonatal Brain Development. *Toxicol. Sci.* **2002,** *67,* 98–103.
9. Viberg, H.; Fredriksson, A.; Eriksson, P. Neonatal Exposure to Polybrominated Diphenyl Ether (PBDE 153) Disrupts Spontaneous Behavior, Impairs Learning and Memory, and Decreases Hippocampal Cholinergic Receptors in Adult Mice. *Toxicol. Appl. Pharm.* **2003,** *192,* 95–106.
10. Meerts, I. A. T. M.; van Zanden, J. J.; Luijks, E. A. C.; van Leeuwen-Bol, I.; Marsh, G.; Jakobsson, E.; Bergman, A.; Brouwer, A. Potent Competitive Interactions of Some Brominated Flame Retardants and Related Compounds with Human Transthyretin In Vitro. *Toxicol. Sci.* **2000,** *56,* 95–104.
11. Chen, G. S.; Bunce, N. J. Polybrominated Diphenyl Ethers as Ah Receptor Agonists and Antagonists. *Toxicol. Sci.* **2003,** *76,* 310–320.
12. von Meyerinck, L.; Hufnagel, B.; Schmoldt, A.; Benthe, H. F. Induction of Rat Liver Microsomal Cytochrome-P-450 by the Pentabromo Diphenyl Ether Bromkal-70 and Half-Lives of Its Components in the Adipose Tissue. *Toxicology* **1990,** *61,* 259–274.
13. Norris, J. M.; Kociba, R. J.; Schwetz, B. A.; Rose, J. Q.; Humistone, C. G.; Jewett, G. L.; Gehring, P. J.; Mailhes, J. B. Toxicology of Octabromobiphenyl and Decabromodiphenyl Oxide. *Environ. Health Persp.* **1975,** *11,* 153–161.
14. Antignac, J. P.; Cariou, R.; Zalko, D.; Berrebi, A.; Cravedi, J. P.; Maume, D.; Marchand, P.; Monteau, F.; Riu, A.; André, F.; Le Bizec, B. Exposure Assessment of French Women and Their Newborn to Brominated Flame Retardants: Determination of Tri- to Deca-Polybromodiphenylethers (PBDE) in Maternal Adipose Tissue, Serum, Breast Milk, and Cord Serum. *Environ. Pollut.* **2009,** *157,* 164–173.
15. Schecter, A.; Pavuk, M.; Papke, O.; Ryan, J. J.; Birnbaum, L.; Rosen, R. Polybrominated Diphenyl Ethers (PBDEs) in U.S. Mothers' Milk. *Environ. Health Persp.* **2003,** *111,* 1723–1729.
16. Takasuga, T.; Senthilkumar, K.; Takemori, H.; Ohi, E.; Tsuji, H.; Nagayama, J. Impact of Fermented Brown Rice with *Aspergillus oryzae* (FEBRA) Intake and Concentrations of Polybrominated Diphenylethers (PBDEs) in Blood of Humans from Japan. *Chemosphere* **2004,** *57,* 795–811.
17. Thomas, G. O.; Wilkinson, M.; Hodson, S.; Jones, K. C. Organohalogen Chemicals in Human Blood from the United Kingdom. *Environ. Pollut.* **2006,** *141,* 30–41.
18. Stanley, J. S.; Cramer, P. H.; Thornburg, K. R.; Remmers, J. C.; Breen, J. J.; Schwemberger, J. Mass-Spectral Confirmation of Chlorinated and Brominated Diphenylethers in Human Adipose Tissues. *Chemosphere* **1991,** *23,* 1185–1195.
19. Cariou, R.; Antignac, J. P.; Marchand, P.; Berrebi, A.; Zalko, D.; André, F.; Le Bizec, B. New Multiresidue Analytical Method Dedicated to Trace Level Measurement of Brominated Flame Retardants in Human Biological Matrices. *J. Chromatogr. A* **2005,** *1100,* 144–152.
20. Mörck, A.; Hakk, H.; Örn, U.; Klasson-Wehler, E. Decabromodiphenyl Ether in the Rat: Absorption, Distribution, Metabolism, and Excretion. *Drug Metab. Dispos.* **2003,** *31,* 900–907.
21. Riu, A.; Cravedi, J. P.; Debrauwer, L.; Garcia, A.; Canlet, C.; Jouanin, I.; Zalko, D. Disposition and Metabolic Profiling of [C-14]-Decabromodiphenyl Ether in Pregnant Wistar Rats. *Environ. Int.* **2008,** *34,* 318–329.
22. Jansen, H. T.; Cooke, P. S.; Porcelli, J.; Liu, T. C.; Hansen, L. G. Estrogenic and Antiestrogenic Actions of PCBs in the Female Rat—In Vitro and In Vivo Studies. *Reprod. Toxicol.* **1993,** *7,* 237–248.
23. Cooke, P. S.; Zhao, Y. D.; Hansen, L. G. Neonatal Polychlorinated Biphenyl Treatment Increases Adult Testis Size and Sperm Production in the Rat. *Toxicol. Appl. Pharm.* **1996,** *136,* 112–117.
24. Stoeckli, M.; Chaurand, P.; Hallahan, D. E.; Caprioli, R. M. Imaging Mass Spectrometry: A New Technology for the Analysis of Protein Expression in Mammalian Tissues. *Nat. Med.* **2001,** *7,* 493–496.
25. Guerquin-Kern, J. L.; Wu, T. D.; Quintana, C.; Croisy, A. Progress in Analytical Imaging of the Cell by Dynamic Secondary Ion Mass Spectrometry (SIMS microscopy). *Biochim. Biophys. Acta* **2005,** *1724,* 228–238.
26. Pacholski, M. L.; Winograd, N. Imaging with Mass Spectrometry. *Chem. Rev.* **1999,** *99,* 2977–3005.
27. Davies, N.; Weibel, D. E.; Blenkinsopp, P.; Lockyer, N.; Hill, R.; Vickerman, J. C. Development and Experimental Application of a Gold Liquid Metal Ion Source. *Appl. Surf. Sci.* **2003,** *203,* 223–227.
28. Touboul, D.; Halgand, F.; Brunelle, A.; Kersting, R.; Tallarek, E.; Hagenhoff, B.; Laprévote, O. Tissue Molecular Ion Imaging by Gold Cluster Ion Bombardment. *Anal. Chem.* **2004,** *76,* 1550–1559.
29. Sjövall, P.; Lausmaa, J.; Johansson, B. Mass Spectrometric Imaging of Lipids in Brain Tissue. *Anal. Chem.* **2004,** *76,* 4271–4278.
30. Touboul, D.; Kollmer, F.; Niehuis, E.; Brunelle, A.; Laprévote, O. Improvement of Biological TOF-SIMS Imaging with a Bismuth Cluster Ion source. *J. Am. Soc. Mass Spectrom.* **2005,** *16,* 1608–1618.
31. Weibel, D.; Wong, S.; Lockyer, N.; Blenkinsopp, P.; Hill, R.; Vickerman, J. C. A C60 Primary Ion Beam System for Time of Flight Secondary Ion Mass Spectrometry: Its Development and Secondary Ion Yield Characteristics. *Anal. Chem.* **2003,** *75,* 1754–1764.
32. Brunelle, A.; Laprévote, O. Recent Advances in Biological Tissue Imaging with Time-of-Flight Secondary Ion Mass Spectrometry: Polyatomic Ion Sources, Sample Preparation, and Applications. *Curr. Pharm. Design* **2007,** *13,* 3335–3343.
33. Brunelle, A.; Laprévote, O. Lipid Imaging with Cluster Time-of-Flight Secondary Ion Mass Spectrometry. *Anal. Bioanal. Chem.* **2009,** *393,* 31–35.
34. Touboul, D.; Roy, S.; Germain, D. P.; Chaminade, P.; Brunelle, A.; Laprévote, O. MALDI-TOF and Cluster-TOF-SIMS Imaging of Fabry Disease Biomarkers. *Int. J. Mass Spectrom.* **2007,** *260,* 158–165.
35. Mas, S; Touboul, D.; Brunelle, A.; Aragoncillo, P.; Egido, J.; Laprévote, O.; Vivanco, F. Lipid Cartography of Atherosclerotic Plaque by Cluster-TOF-SIMS Imaging. *Analyst* **2007,** *132,* 24–26.
36. Tahallah, N.; Brunelle, A.; De La. Porte, S.; Laprévote, O. Lipid Mapping in Human Dystrophic Muscle by Cluster-Time-of-Flight Secondary Ion Mass Spectrometry Imaging. *J. Lipid Res.* **2008,** *49,* 438–454.
37. Debois, D.; Bralet, M. P.; Le Naour, F.; Brunelle, A.; Laprévote, O. In Situ Lipidomic Analysis of Nonalcoholic Fatty Liver by Cluster TOF-SIMS Imaging. *Anal. Chem.* **2009,** *81,* 2823–2831.
38. Seyer, A.; Einhorn, J.; Brunelle, A.; Laprévote, O. Localization of Flavonoids in Seeds by Cluster Time-of-Flight Secondary Ion Mass Spectrometry Imaging. *Anal. Chem.* **2010,** *82,* 2326–2333.
39. Nygren, H.; Börner, K.; Hagenhoff, B.; Malmberg, P.; Månsson, J. E. Localization of Cholesterol, Phosphocholine, and Galactosylceramide in Rat Cerebellar Cortex with Imaging TOF-SIMS Equipped with a Bismuth Cluster Ion Source. *Biochim. Biophys. Acta* **2005,** *1737,* 102–110.
40. Börner, K.; Nygren, H.; Hagenhoff, B.; Malmberg, P.; Tallarek, E.; Månsson, J. E. Distribution of Cholesterol and Galactosylceramide in Rat Cerebellar White Matter. *Biochim. Biophys. Acta* **2006,** *1761,* 335–344.
41. Malmberg, P.; Börner, K.; Chen, Y.; Friberg, P.; Hagenhoff, B.; Månsson, J. E.; Nygren, H. Localization of Lipids in the Aortic Wall with Imaging TOF-SIMS. *Biochim. Biophys. Acta.* **2007,** *1771,* 185–195.
42. Pernber, Z.; Richter, K.; Månsson, J. E.; Nygren, H. Sulfatide with Different Fatty Acids Has Unique Distributions in Cerebellum as Imaged by Time-of-Flight Secondary Ion Mass Spectrometry (TOF-SIMS). *Biochim. Biophys. Acta* **2007,** *1771,* 202–209.
43. Nygren, H.; Malmberg, P. High Resolution Imaging by Organic Secondary Ion Mass Spectrometry. *Trends Biotechnol.* **2007,** *25,* 499–504.

44. Vickerman, J. C. TOF-SIMS—an Overview. In *TOF-SIMS-Surface Analysis by Mass Spectrometry*; Vickerman, J. C., Briggs, D., Eds.; Surface Spectra and IM Publications: Manchester and Chichester, 2001; p.1–40.
45. Sodhi, R. N. S. Time-of-Flight Secondary Ion Mass Spectrometry (TOF-SIMS): Versatility in Chemical and Imaging Surface Analysis. *Analyst* **2004,** *129,* 483–487.
46. Ross, P.; De Swart, R.; Addison, R.; Van Loveren, H.; Vos, J.; Osterhaus, A. Contaminant-Induced Immunotoxicity in Harbor Seals: Wildlife at Risk? *Toxicology* **1996,** *112,* 157–169.
47. Ross, P. S.; de Swart, R. L.; van der Vliet, H.; Willemsen, L.; de Klerk, A.; van Amerongen, G.; Groen, J.; Brouwer, A.; Schipholt, I.; Morse, D. C.; van Loveren, H.; Osterhaus, A. D. M. E.; Vos, J. G. Impaired Cellular Immune Response in Rats Exposed Perinatally to Baltic Sea Herring Oil or 2,3,7,8-TCDD. *Arch. Toxicol.* **1997,** *71,* 563–574.
48. Yuan, W.; Wang, X. N.; Greenwald, G. S. Follicle-Stimulating-Hormone, Human Chorionic-Gonadotropin, and Prolactin Receptors in Hamster Corpora Lutea or Dispersed Luteal Cells During Pregnancy. *Biol. Reprod.* **1995,** *52,* 313–319.
49. Bredhult, C.; Bäcklin, B. M.; Olovsson, M. Effects of Some Endocrine Disruptors on the Proliferation and Viability of Human Endometrial Endothelial Cells In Vitro. *Reprod. Toxicol.* **2007,** *23,* 550–559.